Transient characteristics of Frequency and Damping Factor for Cantilever investigated with Optical Heterodyne Method having high performances

Masao Hirano and Yukari Hirano

Photon Probe, Inc. Development Laboratory, Yoriimachi Saitamaken, 369-1236, Japan

E-mail: photon@m2.hinocatv.ne.jp

The transient characteristics in the damping oscillation of the regular sized cantilever were investigated experimentally with an optical heterodyne displacement meter having the resolutions of 1 nm, 1 μs, and the sequence measurement points of 10^6. The transient results had the peculiarity that neither the vibration frequency nor the damping factor was constant in the measuring time of about several tens of seconds, and that they depended on both the vibration amplitude and the cantilever length. By analyzing results, we obtained some experimental expressions for the frequency and the damping factor. The cantilever length dependence of the frequency was different largely from the Bernoulli-Euler (BE) theory. By introducing and discussing the equation modified the BE equation, we understood the differences with reasonability and consistency. These analyses pointed out that two factors defined in the equation was necessary to express the damping oscillation explicitly and consistently.

1. Introduction

For a cantilever, a miniature or a micro size types have been investigated mainly. These types are developed to atomic force microscope etc. While, for a regular size type, several theories and experiments have been published[1-8] but transient behaviors of the damping factor and the frequency have not been investigated circumstantially. These papers were discussed about the frequency characteristics with various techniques in which they developed with some static values of physical constants. However, they did not explain the damping factor and other characteristics because they did not examine under high precision measurement. The high precision analyses for the damping phenomena will need many transient data having a high signal/noise (S/N) ratio, a high time resolution, and a high displacement resolution. Though many transient measurements were shown[9-11], the resolutions and/or the S/N ratio were not sufficient to practice the high precision analyses.

In general, for a transient measuring method of the vibration, the following optical measurement methods have been proposed, discussed, and reported experimentally, the heterodyne[6,12-15], the homodyne[17-18], the Doppler[19-21], and the other ways. However, these measurements were not enough to discuss the damping factor and the frequency behaviors on the properties of recording points and space-time resolutions. Therefore, to analyze exactly the transient phenomenon, we can know that both of (1) large number of measuring points having small time interval which leads to high time resolution and (2) high displacement resolution need in the continuous measurement.

In addition, to investigate the vibration characteristics, some papers have been reported in the two dimensional measurement[12,19,22,23]. However, the transient data for the damping factor and the frequency were not shown because they have not sufficient S/N ratio and resolutions. On the points of optical detections and data processing, these two-dimensional measurements did not detect with a sufficient optical power per measuring point. Therefore, for analyzing the transient behavior of the cantilever vibration, we judge that the two-dimensional measurement is unsuitable just to get data with high precision.

To respond these requirements, we developed a displacement measuring instrument based on the optical heterodyne method[24] to check transient phenomena clearly, which has enough characteristics of 1 μs time resolution, 1 nm displacement resolution, and 10^6 continuous measuring points to get high precision. By analyzing these measured data, we

discuss transient characteristics of the damping factor and the frequency in the cantilever motion. It is the purpose of this paper to study dynamical characteristics of the cantilever vibration experimentally and theoretically.

Against a frequency's transient behavior in the regular sized cantilever motion, none of report has been discussed in published papers or books including the Bernoulli-Euler theory[25] (BE theory; as a clipped form).

For the transient behaviors on the damping oscillation[26], we will propose the following inference. When a metal is distorted, the atomic bond length and the bond angle within the metallic bond are changed as a function of time in the metal distortion strength. The repeating distortions stock and release their distortion energies repeatedly as a function of the bond factors and time. The bond distortions also bring some corresponded restorative forces. The swings of energies and the swings of forces are producing, and the vibration is accompanying energy dissipations continually. The swings and the dissipations contribute largely to the transient behavior of the damping factor and the frequency. In other words, they will depend on the dynamic characteristics of the metallic-bond induced by a distortion. The distortion is in proportion to the vibration amplitude. Therefore, both the damping factor and the frequency will be affected by the vibration amplitude and they will shift timely because the amplitude decreases timely. This is our inference. To check the validity of the inference will be also our purpose throughout a study in near future.

2. Experiment

To analyze a transient phenomenon, we developed a displacement meter based on the optical heterodyne method. The meter is constituted with a probe and a console as shown in Fig. 1 and its main specifications are listed in Table 1. The stabilized frequency HeNe laser light is divided into two lights (signal and reference lights) and they are shifts their frequency with acousto-optic modulators (AOMs). Both lights are transferred to the probe through polarization maintaining fibers covered with a flexible metal jacket. The signal light is outputted for the sample. The outputted light has characteristics of TEM00, linear polarization, about 150 μW, about 1.1 mrad beam divergence, and about 0.6 mm diameter as a collimated light. The outputted light reflects at the sample and the reflection light is caught by the probe again. The caught light is interfered with the reference light in the

probe. The interference produces an optical beat signal. The probe has two sets of interferometers. The other interferometer produces a reference beat signal with the reference light and the signal light which does not output externally. Both optical beat signals are detected with the respective avalanche photo diodes (APDs) through multi-mode fibers covered with the flexible metal jacket, and are changed to the respective electric signals. The electric signals' frequencies are set to about 2.5 MHz.

By detecting a phase difference between these electric signals and by processing the difference, we obtained a displacement of the sample by the heterodyne method rule in a processing circuit. In the calculation, the resolution is determined mainly by S/N ratios of the beat signals, a stability of laser frequency, and a stability of beat frequency.

To get high resolution, we introduced, APDs, a stabilized frequency HeNe laser having the frequency stability of $\Delta f / f = 3 \times 10^{-9}$, and a frequency shifter having the beat frequency stability of $\Delta f / f = 5 \times 10^{-6}$. As a result, the resolution of displacement is 1 nm or less. In addition, the calculation is executed at 1 μs intervals, therefore, the time resolution is 1 μs. The displacement data are stored up in memories (maximum data points $=10^6$) continuously at intervals of a sampling time which can be selected with an integer multiple of 1 μs. These calculated data are transferred to a personal computer (PC) and analyzed with our original programs based on the heterodyne theory and the least square method. All data are recorded transiently with a format of digital data on the PC expressed with 32 bit.

<<Insert Table I in this point>>

<<Insert Fig.1 in this point>>

The cantilever's surface was polished flatly and smoothly. Therefore, the reflected lights were kept their beam characteristics and scattered hardly. In addition, as the cantilever's size was much larger than the vibration amplitude, all of yawing and rolling were ignored. In the optical circuit, S/N ratios of the beat signals were affected mainly by the reflection light noises, the fluctuations of the optical lengths, the rotations of the light

polarization angle, and the vibrations of the fibers. To suppress these influences, we fixed tightly the fibers and the probe, and controlled the flow of air and the temperature fluctuation, and checked all of noise sources including used instruments.

The experimental setup is shown in Fig. 2. The signal light was outputted for the side of the cantilever. The distance between the probe and the cantilever was about 1 cm. The light reflection point (measurement position) was set at the center position of the width with a distance of 8 mm from the tip of the sample regardless of the sample length. The probe and the cantilever's holder were fastened with stages, holders, and metallic frames to suppress influences of external vibrations and sound noises. All of stages and frames were set on a strongly made table in a tent which is formed with sheets of a polyvinyl film to get suppression of temperature fluctuations within the measurement time. In addition, the tent, all measuring devices, and all instruments excluding PC were set up within a simple shelter built with boards and insulators which were not represented in Fig. 2..

<<Insert Fig.2 in this point>>

The environmental condition parameters of temperature, atmospheric pressure, and humidity, were not controlled because they would not fluctuate within the measurement time (several ten seconds at most) by the effects of the shielding and the covering. They varied within the ranges from 13 to 22 ℃, from 997 to 1009 hPa, and from 35 to 59 %. Even if the temperature changed by 10 ℃, the measuring error of the cantilever length is only 0.02 mm for the length of 100 mm. The error is too small to evaluate the cantilever length dependence. Therefore, our controlling plan will have no problem.

The characteristics of the sample are listed in Table Ⅱ. The vibration was happened by being tapped on the cantilever at near the tip end with a rubber stick. After waiting few seconds, the measurement was started. The tapping force and the waiting time were changed under the various conditions repeatedly. Since the vibration amplitude is about 400 μm at most and the tapping force is much less than the cyclic stress sensitivity limit, the sample is not affected by the stress and strain history. In addition, this small deformation will point out that the strain is kept under the elastic limit of the sample and any plastic deformations never be occurred. So, the measurements always showed very high reproducibility. The length of the cantilever (from the tip to the fixed point) was

changed by moving the fixed point and was measured with accuracy to ±0.05 mm.

<<Insert Table Ⅱ in this point>>

An output time interval of the data (sampling time) was set to 16 or 32 μs because the vibration was too slow to use directly the meter's time resolution and the analysis would need about 1000 output data points for every oscillation period. As the measurement data are calculated every 1 μ s, one output datum was averaged per 16 or 32 measuring points. For every measurement, a million output data were memorized automatically and continuously, so the measurement time was 16 or 32 seconds.

The 10^6 output data were divided to 20 sections and every section was analyzed with the method of least squares independently. The following fitting curve is given by,

$$\begin{aligned} S(k) = \sum_{n=1}^{50000} [& data(k,n) - \{A(k) + E(k)\cdot t_n \\ & + B_1(k)\exp(-\gamma_1(k)\cdot t_n)\cdot\sin((2\pi f_1(k) - \kappa_1(k)\cdot t_n)\cdot t_n + \phi_1(k)\} \\ & + B_2(k)\exp(-\gamma_2(k)\cdot t_n)\cdot\sin((2\pi f_2(k) - \kappa_2(k)\cdot t_n)\cdot t_n + \phi_2(k)\} \\ & + B_3(k)\exp(-\gamma_3(k)\cdot t_n)\cdot\sin((2\pi f_3(k) - \kappa_3(k)\cdot t_n)\cdot t_n + \phi_3(k)\}]^2 \end{aligned} \quad (1)$$

where n, k, and t_n is output data number, section number, and time at the output data number, respectively. And, A (base factor), E (inclination factor), B_i (vibration amplitude ; i=1, 2, 3), γ_i (damping factor ; i=1, 2, 3), f_i (frequency ; i=1, 2, 3), κ_i (frequency shift factor ; i=1, 2, 3), and ϕ_i (initial phase ; i=1, 2, 3) are fitting parameters. And $data(k,n)$ is output datum corresponded to parameters k and n. The optimum values of these parameters were gotten by repeating the fitting operation. After repeated operation, we made the standard deviations of the differences between the output data and the fitting curve decrease to around 10 nm for almost all operations. When the standard deviation was over 30 nm, we excluded the fitting data from the analyses because we judged that unknown noises or unknown vibrations were too large to get an exact result. Even if the vibration amplitude was less than 1 μ m, the standard deviation was saturated at about 4 nm. This saturation limit will be probably happened by the environmental noise generated in the laboratory. As a result of the fitting operation, three frequencies were

almost the same. Moreover, the contributions of higher harmonic wave (especially third and fifth harmonics) were checked by introducing the relations of $f_2 = 3f_1$ and $f_3 = 5f_1$. This fitting analyses gave the relations, $B_2 < 0.0001B_1$ and $B_3 < 0.0001B_1$ for all data. So we concluded that the fundamental wave in the vibration is so strong that all of higher harmonic waves are ignored. In the following description, every parameter is represented without suffix because only the fundamental mode wave behavior is treated.

3. Experimental result

The displacements at the measuring point were measured and registered at the sampling time intervals continuously. As the number of data points is 10^6, one measurement includes several thousands of vibration waves. The damping oscillation's characteristics were gotten with two operations. (1) The damping factor was recognized by analyzing the envelope of data. (2) The frequency was obtained by fitting operation after magnifying a portion of data. The displacement in one measurement varied about from 100 nm to 400 μ m. An example of the measurement data is shown in Figs. 3(a) and 3(b), in which transverse and vertical axes are time in seconds and displacement in nm, respectively.

<<Insert Fig. 3(a) in this point>>

In Fig. 3(a), any oscillation cannot be recognized at all. However the envelope of the curve is decayed. Therefore, a damping phenomenon was observed clearly. By magnifying the transverse axis of Fig. 3(a), an oscillation was recognized and the sine wave was confirmed as shown at Fig. 3(b). The graph shows that the frequency is 71.229 Hz and the noise is very small (i.e. high S/N ratio). Therefore, we can judge that measuring oscillation is a damped sine-wave oscillation. The damping oscillations were observed in all experiments.

<<Insert Fig.3(b) in this point>>

One transient recorded data was divided to 20 sections evenly (each section have 50000 points). We analyzed the vibration characteristics for every section independently. For the frequency, the error was within ±0.004 Hz at worst because about 50 waves were included

in one section at least and one wave was expressed with about 1000 data points. For the damping factor γ, the error $\Delta\gamma$ satisfied the relation of $\Delta\gamma/\gamma \leq 0.02$ for all data because the decay rate was analyzed with about 50 points or more per section.

3.1 Frequency characteristics

3.1.1 Transient characteristics

By doing the fitting operation for all sections independently, we obtained the frequency f and the damping factor γ for each section. Both of f and γ have 20 data lined up at the section interval which is one-twentieth of the sampling time. The series of data show a time dependence of them and give their transient characteristic. In other words, the transient behavior of f can be expressed with the variation of the vibration amplitude B because it is also a transient characteristic. An example is shown in Fig. 4. In the figure, the linear relation of $f = f_0 + m\sqrt{B}$ is satisfied. (A linear equation is shown as a result using the least square method. The constant R^2 is Pearson's correlation coefficient given by the values, $R^2 = 1 - SE \times (SS)^{-1}$, $SE = \sum (Y_i - y_i)^2$, and $SS = (\sum y_i^2 - (\sum y_i)^2) \times N^{-1}$, where y_i, Y_i, and N are the i-th data value (frequency), the i-th calculated value on the linear equation, and the number of data, respectively. (Expressions of the linear equation (or the cubic curve) and the R^2 value are used for almost figures in this paper.)

Some characteristics are known, (1) the frequency is not constant but increases with time, (2) the frequency shift is very small but is larger than our experimental resolution (every data have noises of ±0.004 Hz or less), (3) there are a linear relation between the vibration amplitude and the frequency. These transient characteristics were observed in all measurements. We reflected in advance the shift effect to the fitting operation by introducing the factor of κ as given in Eq. (1).

<<Insert Fig.4 in this point>>

For the first and second notice, the measuring error and analyzing error is so small that the frequency shifts and their vibration amplitude dependences were confirmed with good reproducibility significantly. In other words, a result of “the decrease of the vibration amplitude makes the frequency increase” was confirmed for all experiments.

For the third notice, the fitting with a linear function of $f = f_0 + m\sqrt{B}$ had always high correlation coefficient. But, in sometime cases, the fitting with a cubic function of $f = f_0 + a_3 B^{3/2} + a_2 B + a_1 B^{1/2}$ was better slightly than one with the linear function. However these R^2 values were nearly equal. So we adopted the linear function as the fitting curve. The condition of $m < 0$ were always satisfied. In addition, by repeating experiments, it was certified that these parameters didn't depend on the initial vibration amplitude and the sampling time.

The reproducibility of these results was within about an error of ±0.2 % in spite of all effects based on the variations of the temperature, the atmospheric pressure, and the humidity.

3.1.2 Dependence of f_0 on the cantilever length

By varying the cantilever length L from 75 mm to 200 mm, we investigated the dependence of f_0 (the frequency at zero vibration amplitude) on L as shown at Fig. 5. The value of $\log(f_0)$ depended linearly on $\log(L)$ with very high R^2 of 0.998. As a result, we got the relation of $f_0 \propto L^{-1.863}$. While, the BE theory gives the relation of $f \propto L^{-2}$. Though f_0 is not a measurement value, as the relation of $f_0 >> -m\sqrt{B}$ is always satisfied, we may represent the relation of $f \propto L^{-1.863}$, with which we obtain that the L dependence of the frequency is different from one of the BE theory explicitly.

<<Insert Fig.5 in this point>>

To study the difference between the experimental results and the BE theory in Section 4, the relation of $f_0 \propto L^{-1.863}$ was examined analytically with terms up to the higher order of L as follows. The relation form will be developed by the following expressions, (1) $D(\frac{1}{L^2} + \frac{d}{L})$, (2) $D(\frac{1}{L^2} - \frac{d}{L^3})$, (3) $D(\frac{1}{L^2} - \frac{d}{L^4})$, (4) $\frac{D}{L^2 + d}$, (5) $\frac{D}{L^2 + dL}$, etc. The case of (1) is denied by the BE theory. For the cases (4) and (5), the expansions are corresponded to cases (2) and (3) approximately. Therefore, as the experimental expression of f_0, we

adopted both cases (2) and (3). By fitting to the data curve, we obtained the values of D and d as shown in the Table Ⅲ. In the fitting process, the correlation coefficient between data and the expression always kept over 0.995. It shows that these expressions consist of the sum of the BE theory's term and an additional term. Though the additional terms in two cases are difference, in this stage, we could not select with explicit belief. Therefore we propose both cases as the experimental expression of f_0 and f.

<<Insert Table Ⅲ in this point>>

3.1.3 Dependence of m on the cantilever length

The slope m depend also on the cantilever length. Though the analytical error was not small, the relation of $m \propto L^{-3.5}$ was obtained as shown in Fig 6 (the longitudinal axis is $\log(-m)$ because $m < 0$). Though the linear relation was appropriate for the most results, the cubic function was sometimes reasonable expression for small L. This slight difference in the expression may make the data distribute as shown in Fig. 6.

<<Insert Fig.6 in this point>>

The L dependence of m is different obviously from one of the frequency. The difference may suggest that the generation mechanism of m is different from one of the frequency. However, the frequency shift $m\sqrt{B}$ is so small that both f and f_0 will be generated by the same mechanism. Therefore, the term of $m\sqrt{B}$ will have the same L dependence as the frequency because it is an additional frequency shift $\Delta f_0 = f - f_0$. By treating the experimental expressions of the frequency described in Sec. 3.1.2, we can estimate that either state of $m\sqrt{B} \propto L^{-3}$ or $m\sqrt{B} \propto L^{-4}$ will be satisfied. The estimation is matched to the experimental expression of $m \propto L^{-3.5}$ if the vibration state is formed in a mixture of two states which correspond to two cases in table Ⅲ.

This mixture may be understood with the following approach. The vibration is originated in a repeated energy-exchange operation between distortion energy and kinetic energy accompanying dissipations of heat energy. The states will be able to be described with behaviors (include their time dependences) of these energies induced by each

mechanism. So, if two states correspond to the relations of $m\sqrt{B} \propto L^{-3}$ and $m\sqrt{B} \propto L^{-4}$, two states have different energy behaviors and mechanisms. However, when total energy is nearly the same between two states, the two states can generate competitively. The competitive generation process will change the L dependence to a characteristics of a middle state described as a mixed state of two states. Therefore, we can understand the experimental results of L dependence by introducing the mixture of two states.

3.2 Damping factor characteristics

3.2.1 Transient characteristics

The damping factor γ was also investigated individually for all sections and its transient variation was represented as a function of the vibration amplitude. An example is shown in Fig. 7, which is plotted at the section intervals for the transverse axis. In this graph, the error of γ was less than 0.003. Explicitly, the damping factor was not constant but depended on the vibration amplitude within the measurement time of several tens seconds. The dependence was complex and γ had a minimum value described with the relation of $\gamma = \gamma_m + \beta(\sqrt{B} - \sqrt{B_m})^N$, where γ_m, B_m, and β are the minimum damping factor, the vibration amplitude at the minimum, and a coefficient, respectively, the value of N was gotten by the fitting. For all data, we obtained N=2 or N=3. The relation $\beta > 0$ was always kept. All of values of γ_m, B_m, and β depended on the cantilever length L. However, they didn't depend on the initial vibration amplitude and the sampling time. Certainly large initial vibration amplitude was produced large damping factor. However, the minimum value was always observed at nearly the same B_m value. The reproducibility was an error of ±2.6 % including all effects based on the variations of the temperature, the atmospheric pressure, and the humidity.

<<Insert Fig.7 in this point>>

The generation of the minimum will be understood as follows. Two kinds of energy, the distortion energy and the kinetic energy, produce the vibration and the decay. When B is large, the distortion is so large that its energy release makes the damping factor enlarge. Larger distortion (i.e. amplitude) brings about large damping. While, when B is small,

the distortion is to be weak and the kinetic energy is dominant for moving cantilever. The air resistance will contribute to the damping mainly. The kinetic energy and the resistance is proportional to B^2 and B, respectively. So, smaller B brings about large damping. Therefore, this counteraction based on two kinds of energy will generate the minimum.

3.2.2 Dependence of γ_m on the cantilever length

The minimum value of the damping factor γ_m depended also on the cantilever length L as shown in Fig. 8. The graph shows that (1) γ_m is not constant, (2) it depends on L, and (3) short L produces large γ_m. The characteristics of (1) and (2) were expected by their transient variations and the previous analyses about the frequency. For the third characteristics, we will be able to understand as follows. Shorter cantilever generates larger distortion under the condition that the vibration amplitude is the same. Larger distortion generates larger restoring force. Larger force generates larger speed of the cantilever and stronger damping. Therefore, shorter cantilever will produce larger damping factor.

<<Insert Fig.8 in this point>>

As the analytical data points were 20 mostly and the error in the curve fitting operation was not small, the value of γ_m distributed widely. Especially, for small L value, the wide fluctuations were brought a indeterminancy for the selection of N. Though these some ambiguities were appeared in the fitting operation, the values of γ_m were expressed with the relation of $\gamma_m \propto L^{-2.5\pm0.1}$ definitely. So we can propose several expressions for γ_m, (1) $G(\frac{1}{L^2}+\frac{g}{L^3})$, (2) $G(\frac{1}{L^2}+\frac{g}{L^4})$, (3) $\frac{G}{L^2-g}$, (4) $\frac{G}{L^2-Lg}$, etc., where G and g are unsettled fitting parameters. Cases (3) and (4) are approximately equal to cases (1) and (2). So, the cases (1) and (2) were used in the following analyses. However, in this stage, we could not judge which cases it was a good expression to understand. Therefore, we treated both cases as the experimental expression and calculated their values as listed in Table Ⅳ.

<<Insert Table Ⅳ in this point>>

3.2.3 β and B_m characteristics

The values of B_m and β depended also on the cantilever length as shown in Figs. 9 and 10, respectively. The error for the damping factor in the neighborhood of the minimum was nearly equal to 0.005. The minimum point as shown in Fig. 7 was detected in almost all cases even if the error was over 0.01. As the calculated points are 20 at most in the fitting curve, the values of B_m and β distribute widely. For both graphs, though the dispersions were not so small, both parameters could be represented with expressions of $B_m \propto L^{1.9\pm0.5}$ and $\beta \propto L^{-4.9\pm0.2}$. In spite of the wide distributions, the signs of the slopes were different obviously between these two fitting lines.

<<Insert Fig.9 in this point>>
<<Insert Fig.10 in this point>>

The difference of the slope sign will be understood as follows. Two kinds of energy will control the damping as described in Sec. 3.1.2. When L is large, the distortion energy is weak because the bending curvature is to be small and, therefore, the damping is small. So, large vibration amplitude needs to get the condition that the distortion energy works dominantly. The variation of the kinetic energy loss is not so large. Therefore, large L makes B_m increase so that the slope sign in the expression of B_m is positive. And, the decrease of the distortion energy under large L requires a large vibration amplitude to get a balance between the distortion energy and the kinetic energy. In other words, the damping decreases with increasing the cavity length. Therefore, the slope sign in the expression of β is negative. But, we cannot discuss them quantitatively in this paper.

4. Theory

We investigated several equations proposed in many published papers which refer to the damping oscillation. So that, we knew that the following modified Bernoulli-Euler equation is the best to understand our experimental results.

$$EI\left(\frac{\partial^4 y}{\partial x^4}+\mu\frac{\partial^5 y}{\partial x^4 \partial t}\right)+\rho A\frac{\partial^2 y}{\partial t^2}+\lambda\frac{\partial y}{\partial t}=0, \qquad (2)$$

where, y, x, t, E, I, ρ, and A are displacement, vibration position, time, Young modulus, second moment of area, density, and cross section, respectively. The factors μ and λ are coefficients of resistances based on the shearing force and the vibration velocity, respectively. The damping phenomenon requires both conditions of $\mu > 0$ and $\lambda > 0$.

To resolve Eq. (2) and to understand the match between this equation and our experimental results, we introduced three assumptions.

<First assumption>

The first assumption is to express the displacement with a separation of variables as follows,

$$y(x,t) = Z(x)\exp(-\gamma t)\sin(\omega t), \tag{3}$$

where γ, ω, and $Z(x)$ are damping factor, angular frequency, and vibration amplitude at position x, respectively. On substituting Eq. (3) in Eq. (2), it follows that,

$$\begin{aligned} &\frac{d^4 Z(x)}{dx^4} - P^4(t)Z(x) = 0 \\ &P^4(t) \equiv \frac{k_2 \sin(\omega t + \phi_2)}{EIk_1 \sin(\omega t + \phi_1)} \end{aligned}, \tag{4}$$

where k_1, k_2, ϕ_1 and ϕ_2 are defined as follows,

$$\begin{aligned} &k_1 = \sqrt{(1-\mu\gamma)^2 + (\mu\omega)^2}, k_2 = \sqrt{(\rho A(\omega^2 - \gamma^2) + \lambda\gamma)^2 + (2\rho A\gamma\omega - \lambda\omega)^2} \\ &\cos\phi_1 = \frac{1-\mu\gamma}{k_1}, \sin\phi_1 = \frac{\mu\omega}{k_1}, \cos\phi_2 = \frac{\rho A(\omega^2 - \gamma^2) + \lambda\gamma}{k_2}, \sin\phi_2 = \frac{2\rho A\gamma\omega - \lambda\omega}{k_2}. \end{aligned}$$

If $P^4(t)$ is not time function and if it is constant, the equation is consistent with the BE theory which gives a condition $PL = 1.875$ for the lowest mode vibration. (The relation $P(t) = 1.875 \times L^{-1}$ will be able to treat as an approximation.)

<Second assumption >

The second assumption is to replace $P^4(t)$ with its time-averaged value Q^4 which is defined as follows,

$$Q^4 = \frac{1}{T}\int_0^T dt P^4(t) = \frac{1}{T}\int_0^T dt \frac{k_2 \sin(\omega t + \phi_2)}{EIk_1 \sin(\omega t + \phi_1)} = \frac{k_2}{EIk_1}\cos(\phi_2 - \phi_1). \tag{5}$$

For the lowest mode, as Q can treat as a constant, the relation of $Q = 1.875 \times L^{-1}$ will be satisfied as the first approximation. By using this approximation and new variables defined

with $\chi \equiv \frac{\rho A}{EIQ^4} = \frac{\rho A}{EIc} L^4 \equiv \chi_0 L^4$, $\delta \equiv \frac{\lambda}{EIQ^4} = \frac{\lambda}{EIc} L^4$, and $c = (1.875)^4$, we get the following smart form,

$$\omega^2 = \frac{1 - 2\gamma\mu - \gamma\delta(1-\gamma\mu)}{\chi(1+\gamma\mu) - \mu(\mu+\delta)}. \tag{6}$$

<Third assumption >

The third assumption is to introduce the L dependence for two parameters λ and μ as follows,

$$\lambda = \lambda_0 \frac{1}{L^N} \quad (\delta = \frac{\lambda}{EIc} L^4 = \frac{\lambda_0}{EIc} L^{4-N} \equiv \delta_0 L^{4-N}) \qquad \text{and} \qquad \mu = \mu_0 L^M .$$

Both λ_0 and μ_0 are constants and both N and M are undetermined values.

With using these assumptions and substituting the experimental expressions of $\omega_0 = 2\pi D(\frac{1}{L^2} - \frac{d}{L^m})$ and $\gamma = G(\frac{1}{L^2} + \frac{g}{L^n})$ (both indexes m and n are 3 or 4) and their values given in Tables Ⅲ and Ⅳ to Eq. (6), we can rewrite under an approximation of $\omega \cong \omega_0$. From the consistent judge for order of L term under the condition of $g << 1$, we could accept conditions, $N = 2$, $M = 2$, and $m = n$. By treating these conditions, the following expressions are satisfied regardless of the value of $m(=n)$. Higher order terms were ignored because they were neglected in the expressions of ω and γ,

$4\pi^2 D^2 = (1 - 2G\mu_0 - G\delta_0 + G^2\mu_0\delta_0)R$ (For L^{-4} term), and

$8\pi^2 D^2 d = Gg(2\mu_0 + \delta_0 - 2G\mu_0\delta_0)R$ (For L^{-2-m} term),

where $R^{-1} = \chi_0(1+G\mu_0) - \mu_0(\mu_0+\delta_0)$. These equations are changed to,

$$\frac{2d}{g} = \frac{2G\mu_0(1-G\delta_0) + G\delta_0}{(1-G\mu_0)(1-G\delta_0) - G\mu_0}$$

$$\frac{4\pi^2 D^2}{G^2} = \frac{(1-G\mu_0)(1-G\delta_0) - G\mu_0}{G^2\chi_0(1+G\mu_0) - G\mu_0(G\mu_0 + G\delta_0)} \tag{7}$$

,

Equations (7) give the values of $G\mu_0$ and $G\delta_0$ (and the other values) uniquely as shown in Table Ⅴ under the conditions of $G\mu_0 > 0$ and $G\delta_0 > 0$.

<< Insert Table Ⅴ in this point>>

These values show that the approximations of $\gamma\mu << 1$ and $\delta >> \mu$ are adequate. The BE theory's frequency for the lowest mode vibration has been expressed with $\omega_{th}^2(L) = \frac{(1.875)^4}{L^4}\frac{EI}{\rho A} = \frac{1}{\chi}$. Therefore, Eq. (6) is rewritten with changing expression from ω^2 to ω_{cal}^2 by

$$\frac{\omega_{cal}^2}{\omega_{th}^2} = \frac{1-\gamma\delta}{1-\mu\delta\omega_{th}^2} \quad . \tag{8}$$

To confirm this relation, experimental frequencies were compared with this theoretical calculation frequency ω_{cal} as shown in Fig. 11. In the expression of ω_{cal}, both of γ and L are used with the experimental data and the parameters in Table Ⅱ and Ⅴ.

<< Insert Fig. 11 in this point>>

This graph shows clearly that the experimental frequency is nearly equal to the theoretical calculation frequency in the wide range of frequency, where the cantilever length is varied from 75 to 200mm. In other words, the cantilever vibration having above length could be expressed with Eq. (8) and the parameters shown in Table Ⅴ.

This equality and Eq. (8) suggest that the proportional relation of $\omega_{\exp}^2 \propto -\kappa(L)\gamma$ is realized, where $\omega_{\exp}$ is the experimental frequency and the coefficient $\kappa(L)$ is a function of L. So the relation has to be confirmed individually under every L. They were checked on for all cantilever length. An example is shown in Fig. 12 in the case of L=140.95 [mm]. Though the data distribution is broad, a linear relation is recognized with a negative slope dependence sufficiently. The characteristics were satisfied for all L and the relation of $\kappa(L) = \frac{\delta\omega_{th}^2}{1-\mu\delta\omega_{th}^2} = const \times \frac{1}{L^2}$ could be expressed with $const = 110 \pm 15$ for all L by using parameters given in Table Ⅱ and Ⅴ

<<Insert Fig.12 in this point>>

Therefore, we can understand the experimental results by introducing Eq. (2) including two resistance parameters and by setting three assumptions. In short, our proposed modified EB equation can be described the damping oscillation of the cantilever.

5. Discussion

(1) The coefficients λ and μ are always appeared in all equations (Eqs. (2)-(8)). It shows that both coefficients are essential factors having correlative effects in the analyses of the damping oscillation. If either of the factors is zero, experimental results cannot understand without the consistency. They don't contribute to the motion independently because they appear as a pair in the functions of the frequency and the damping factor.

(2) The second assumption will be reasonable by the following reason. The time variation of ω and γ is small as shown in Figs. 4 and 7. The coefficients λ_0 and μ_0 are nearly constant as shown in Table Ⅴ. Therefore, parameters in Eq. (4) are estimated to be $k_1 \approx 1$, $k_2 \approx \lambda\omega$, $\cos\phi_1 \approx 1$, $\sin\phi_1 \approx 0$, $\cos\phi_2 \approx 0$, $\sin\phi_2 \approx -1$, $\phi_1 \approx 0$, and $\phi_2 \approx \frac{3\pi}{2}$. Though the function $P^4(t)$ has singular points at $\omega t = 2n\pi$ (n;integer), the contribution to the displacement at the points in the period motion will be small because the cantilever vibration will pass through these points momentary in its continuous movement by its inertial force. Therefore, the second assumption will have acceptability without defect.

(3) The third assumption will be reasonable by the following reason. The expression of ω^2 includes terms of L^{-4}, L^{-5}, and L^{-6} as shown in Table Ⅲ. And χ is expressed with term of L^4. So, the numerator (mainly $\gamma\delta$) in Eq. (6) must include L^{-1}, L^{-2}, and L^{-3} terms. While, the expression of γ include L^{-2} and L^{-3} (or L^{-4}) as shown in Table Ⅳ. Therefore, the term δ ($\propto \lambda L^4$) must be expressed with the term of L^2. The term $\mu(\mu+\delta)$ of the denominator of Eq. (6) is required to express with the term of L^4. Therefore, relations of $\mu \propto L^2$ and $\lambda \propto L^{-2}$ ($\delta \propto L^2$) can be assumed consistently.

(4) For values of m and n in the expressions of ω (Table Ⅲ) and γ_m (Table

Ⅳ), we could not specified except the condition of $m = n$. For both $m = 3$ and $m = 4$ cases, our experimental results could be understood them without contradiction and defectiveness. Reversely, we infer that a damping oscillation may be a behavior fluctuating between two states corresponded to two cases, whose idea is also touched in Sec. 3.1.3.

(5) The ratio of two resistance terms in Eq. (2) on the lowest mode is written by,

$$\frac{EI\mu \dfrac{\partial^5 y}{\partial x^4 \partial t}}{\lambda \dfrac{\partial y}{\partial t}} = \frac{EI\mu_0}{\lambda_0} Q^4 L^4 \cong \frac{EI\mu_0}{\lambda_0} (1.875)^4 \cong 7.8 \times 10^{-7}.$$

The ratio is extremely small. So, the resistance based on the shearing stress may be ignored in Eq. (2). Certainly, the condition of $\mu = 0$ do not happen any problem in Eqs. (3)-(8). So, we have a question "Is the introduction of two terms needful and essential in the discussion of the damping oscillation? ". In the cantilever, the kinetic energy dissipation will be much larger than the shearing stress energy dissipation, and, therefore, the damping oscillation will be controlled strongly by kinetic energy dissipation. The ratio shows as if this view is more suitable. However, Eq. (8) is satisfied as demonstrated in Figs. 11 and 12, and the condition of $\mu = 0$ cannot explain all of experimental results. Therefore, even if the term is small, the two coefficients are needful and indispensable to understand the damping oscillation.

(6) For the experimental results "the frequency and the damping factor depend on the vibration amplitude", we don't have sufficient explanation capability quantitatively. At the present stage, our inference will be investigating to clear only qualitatively the cantilever motion mechanism.

6. Conclusion

The damping oscillations of the cantilever were measured with the optical heterodyne meter which was developed with high performances of a time resolution of 1 μs, a displacement resolution of 1 nm, and continuous measured points of 10^6. The measured data errors were less than about 10 nm at worst. By fitting data to the form written by Eq. (1) with the least square method, we investigated the damping oscillations of the cantilever. We obtained that both the vibration frequency f and the damping factor γ depend on

the vibration amplitude B transiently in the expressions of $f = f_0 + m\sqrt{B}$ and $\gamma = \gamma_m + \beta(\sqrt{B} - \sqrt{B_m})^N$, respectively. In addition, by analyzing many data, we obtained that all these values of f_0, m, γ_m, β, and B_m depend on the cantilever length L. Especially, the relations $f_0 \propto L^{-1.863}$ and $\gamma_m \propto L^{-2.5\pm0.1}$ were obtained.

To understand our results, we investigated the modified BE equation. By analyzing the equation under three assumptions, we could explain the experimental results through emphasizing parameters of λ and μ clearly. We calculated both values with the experimental expressions and the analyzed values. And we conclude that both parameters are necessary and indispensable factors for the description of the damping oscillations.

References

1) Jimbo, Y. and Yamada, S., Vibration of a tuning fork, The Horological Institute of Japan **50,** 1 (1969) [in Japanese].
2) Yamada, S., Kurosaki, S., and Jimbo, Y., The Horological Institute of Japan **75,** 1 (1975**)** [in Japanese].
3) Rossing, T. D., Russell, D. A., and Brown, D. E., Am. J. Phys. **60,** 620 (1992**)**.
4) Bates, L., Beach, T., and Arnott, M., J. Undergraduate Research Phys. **18,** 9 (1999**)**.
5) Sandoz, P., Carry, E. J., Friedt, M., Trolard, B., and Reyes, J. G., Am. J. Phys. **76**, 1 (2008).
6) Gendre, M. F., Haverlag, M., and Krosen, G. W. M., Appl. Phys. **43,** 234004 (2010**).**
7) Shoemaker, R. L., Rev. Phys. Chem. **30,** 239 (1979**)**.
8) Calle, S., Remenleras, J. P., Matar, O. B., Hachemi, M. E., and Patat, F., J. Acoust. Soc. Am. **118,** 2829 (2005**)**.
9) Tamada, N., Fuchino, S., Natori, N., Ishii, I., and Okano, M., Cryogenics **33,** 1023 (1993**)**.
10) Hruschka, R., Park, G., Kleine, H., and O'Byrne, S., Proc. SPIE 26th International Congress on High-Speed imaging and photonics vol.**7126,** 71260J (2009**)**.
11) Tomoda, M., Shiraishi, N., Kolosov, O. V., and Wright, O. B., Appl. Phys. Lett. **82,** 622 (2003**)**.
12) Toida, M., Kondo, M., Ichimura, T., and Inaba, H., Appl. Phys. B **52,** 391 (1991**)**.
13) Valley, J. F., Wu, J. W., and Valencia, C.L., Appl. Phys. Lett. **57,** 1084 (1990**)**.
14) Voheringer, P., and Scherer, N. F., J. Phys. Chem. **99,** 2684 (1995**)**.
15) Silva, D. M., Barbosa, E. A., and Wetter, N.U., Rev. Sci. Instrum. **83,** 103103 (2012**)**.
16) Marques, T. G., Gouveia, A., Pereira, T., Fortunato, J., Carvalho, B. B., Sousa, J. Silva, C., and Fernandes, H., Rev. Sci. Instrum. **79,** 10E711 (2008**)**.
17) Pozar, T., Gregorccic, P., and Mozina, J., Opt. Express **17,** 22906 (2009**)**.
18) Sizgoric, S. and Gundjian, A. A., Proc. IEEE **57,** 1313 (1969**)**.
19) Norgia, M., Donati, S., and Alessandre, D. D., IEEE. J. Quantum Electronic **57,** 800 (2001**)**.
20) Leutenegger, M., Harbi, P., Thacher, T., Raffoul, W., and Lasser, T., AIP Conf. Proc. vol.**1457,** 282 (2012).

21) Longo, R., Steenackers, G., Vaniandult, S., and Guillaume, P., AIP Conf. Proc. Vol. **1253,** 94 (2010**)**.
22) Wong, W. O., Int. J. Eng. Ed. **14,** 241 (1998**)**.
23) Acedo, P., Pedneira, P., Criado, A. R., and Lamele, H., Rev. Sci. Intrum. **79,** 10E713 (2008**)**.
24) Hirano, M., *Optical Heterodyne Measurement Method*, In Handbook of Optical Metrology, ed. T. Yoshizawa (Taylor & Francis/CRC press, New York, 2009**)**, Part 2 Chap. 10.
25) Wylie, C. R., *Advanced Engineering Mathematics* (Mc.Grow-Hill, New York 1966**)**.
26) Goodman, L. E., *Material damping and slip damping*, In Shock and Vibration Handbook, ed. C.M. Harris (Mc.Grow-Hill Handbooks; New York, 1991**)** Chapter 36.

Figure Captions

Fig. 1 Construction of the optical heterodyne meter. Two interferometers in the probe make two optical beat-signals. The phases of the signals are calculated in the processing circuit and are changed to the displacement data.

Fig. 2 Experimental setup. Sample cantilever and the probe were fixed with holders, stages, and frames. The displacement was measured optically with resolution of 1nm.

Fig. 3(a) An example of oscillation on the condition 150.0 mm cantilever length (measurement time=16 s). Thought none of oscillation wave form can be confirmed in this graph, the envelope curve is unquestionably decayed.

Fig. 3(b) The magnification of Fig. 3(a) (range from 15.92 s to 16 s). The oscillation is a sine wave and its frequency is 71.229 ±0.001 Hz. As the noise is less than 10 nm. The damping can hardly be recognized in this graph.

Fig. 4 An example of transient variation of the frequency. The cantilever length is 85.0 mm.

Fig. 5 The cantilever length dependence of f_0. The data were plotted on the relation of $f_0 \propto L^{-1.863}$ with high correlation coefficient of 0.998.

Fig. 6 The cantilever length dependence of the slope m of the relation $f = f_0 + m\sqrt{B}$ (longitudinal axis is $\log(-m)$ because of $m < 0$). The relation $m \propto L^{-3.5}$ was obtained.

Fig. 7 An example of the transient variation of the damping factor γ. The cantilever length was 102.5 mm. It was expressed with the relation of $\gamma = \gamma_m + \beta(\sqrt{B} - \sqrt{B_m})^3$ with high correlation coefficient.

Fig. 8 The cantilever length dependence of γ_m. The relation of $\gamma_m \propto L^{-2.5\pm0.1}$ was obtained.

Fig. 9 The cantilever length dependence of B_m. The relation of $B_m \propto L^{1.9\pm0.5}$ was obtained

Fig. 10 The cantilever length dependence of β. The relation of $\beta \propto L^{-4.9\pm0.2}$ was obtained.

Fig. 11 Conformity between the theoretical frequency and the experimental frequency data. In the wide range, the validity of our induced parameters in Table Ⅴ is also confirmed.

Fig. 12 An example of the relation between γ and ω^2 in the L=140.95 mm case. A

linear relation $\omega^2 \propto -\kappa(L)\gamma$ was nearly satisfied. This negative slope was realized for all cases.

Table I Characteristics of the optical heterodyne displacement meter.

Method	Optical heterodyne measurement method
Displacement resolution	1 nm
Time resolution	1 μs
Laser	Frequency stabilized HeNe laser Frequency stabilization; $\Delta f / f = 3 \times 10^{-9}$
Beat-frequency controller	Frequency shifter Beat frequency stabilization; $\Delta f / f = 5 \times 10^{-6}$
Measurement point	10^6 points
Sampling time	Selection among 1μs, 2μs,4μs, 8μs, 16μs… 2^N μs…2048μs. N is 0 to 11.
Interferometer	Both an outputted signal light and a reference light are interfered in the probe, two optical beat-signals are produced.
Optical Probe size	Cylindrical form. 35 mm diameter, 80 mm length

Table Ⅱ Characteristics of the cantilever sample

Material	SUS304
Size	Cross section $10mm \times 2mm$ Length 300 mm (max.)
Density	7.93×10^3 [kg/m^3]
Young modulus	193 [GPa]

expression	D	d
$f_0 = D(\frac{1}{L^2} - \frac{d}{L^3})$	1.702 ± 0.05	$(1.48 \pm 0.05) \times 10^{-2}$
$f_0 = D(\frac{1}{L^2} - \frac{d}{L^4})$	1.604 ± 0.05	$(9.02 \pm 0.28) \times 10^{-4}$

Table Ⅲ The experimental result $f_0 \propto L^{-1.863}$ could be expressed with terms up to the higher order of L, two cases were proposed. For both cases, the coefficients D and d were calculated analytically by fitting operations.

expression	G	g
$\gamma_m = G(1/L^2 + g/L^3)$	0.00345 ± 0.00014	0.107 ± 0.0125
$\gamma_m = G(1/L^2 + g/L^4)$	0.00482 ± 0.00027	0.00445 ± 0.00045

Table Ⅳ The experimental result $\gamma_m \propto L^{-2.5\pm0.1}$ was able to describe with two experimental expressions in which the coefficients G and g were calculated analytically.

m (=n)	$G\mu_0$	$G\delta_0$	μ_0	δ_0	λ_0
3	$(1.7\pm0.10)\times10^{-7}$	0.22 ± 0.015	$(4.9\pm0.3)\times10^{-5}$	64 ± 4	1020 ± 70
4	$(2.3\pm0.15)\times10^{-7}$	0.28 ± 0.02	$(4.9\pm0.3)\times10^{-5}$	60 ± 4	950 ± 60

Table V The values λ_0 [Kgm/s], μ_0 [s/m^2], δ_0 [s/m^2], and the other factors were calculated with the experimental expressions. The coefficients are nearly constant in spite of different expression.

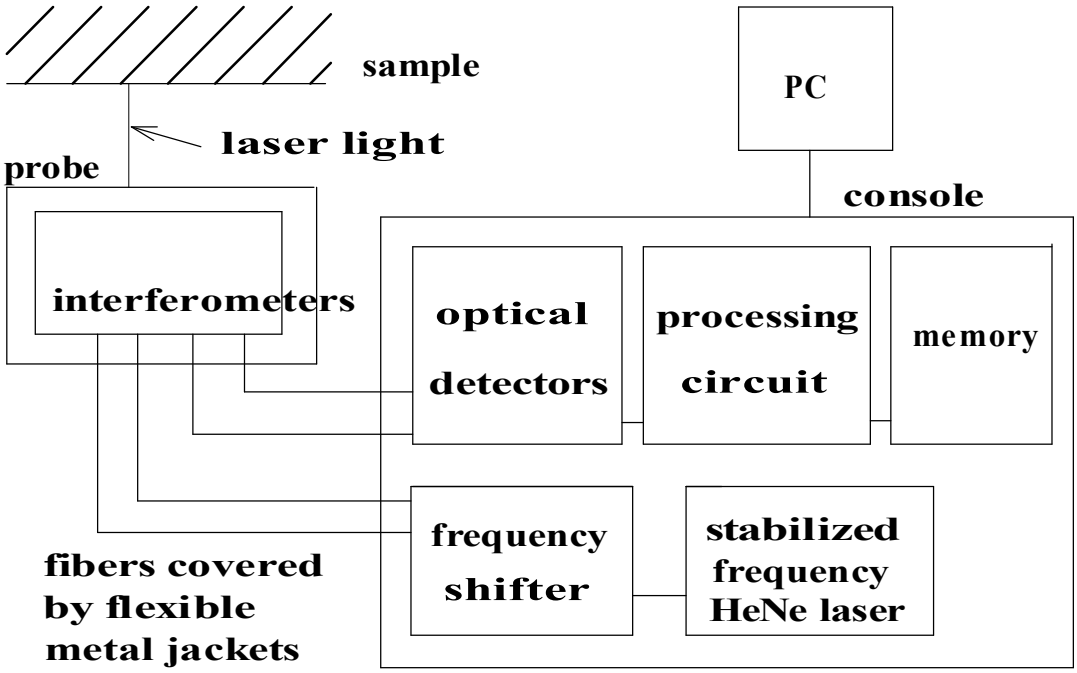
sample
PC
laser light
probe
console
interferometers
optical
detectors
processing
circuit
memory
frequency
shifter
stabilized
frequency
HeNe laser
fibers covered
by flexible
metal jackets

Fig. 1

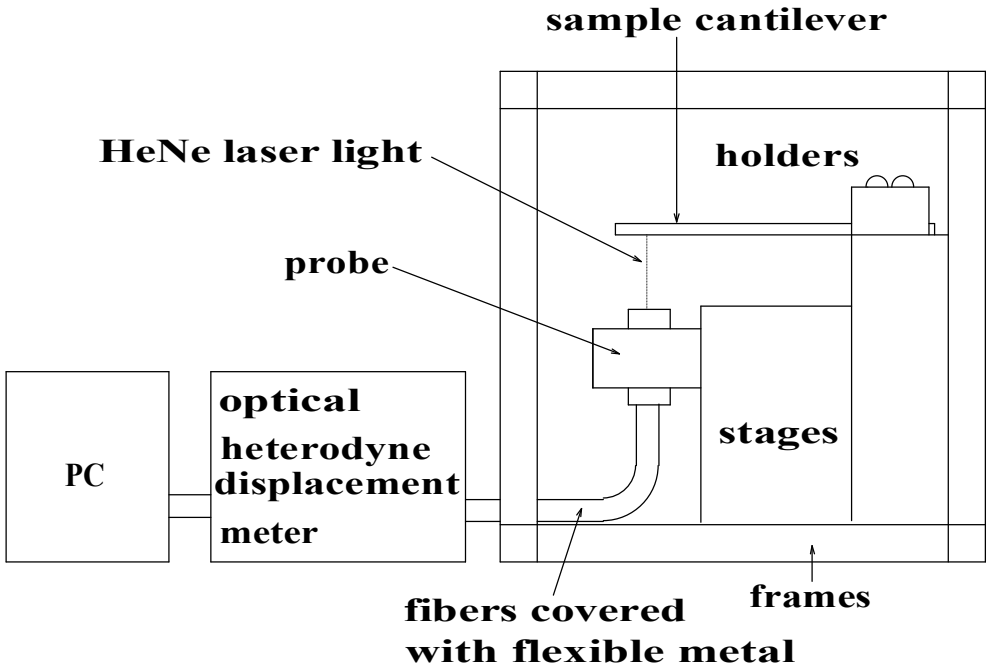
sample cantilever
HeNe laser light
holders
probe
PC
optical
heterodyne
displacement
meter
stages
fibers covered
with flexible metal
frames

Fig. 2

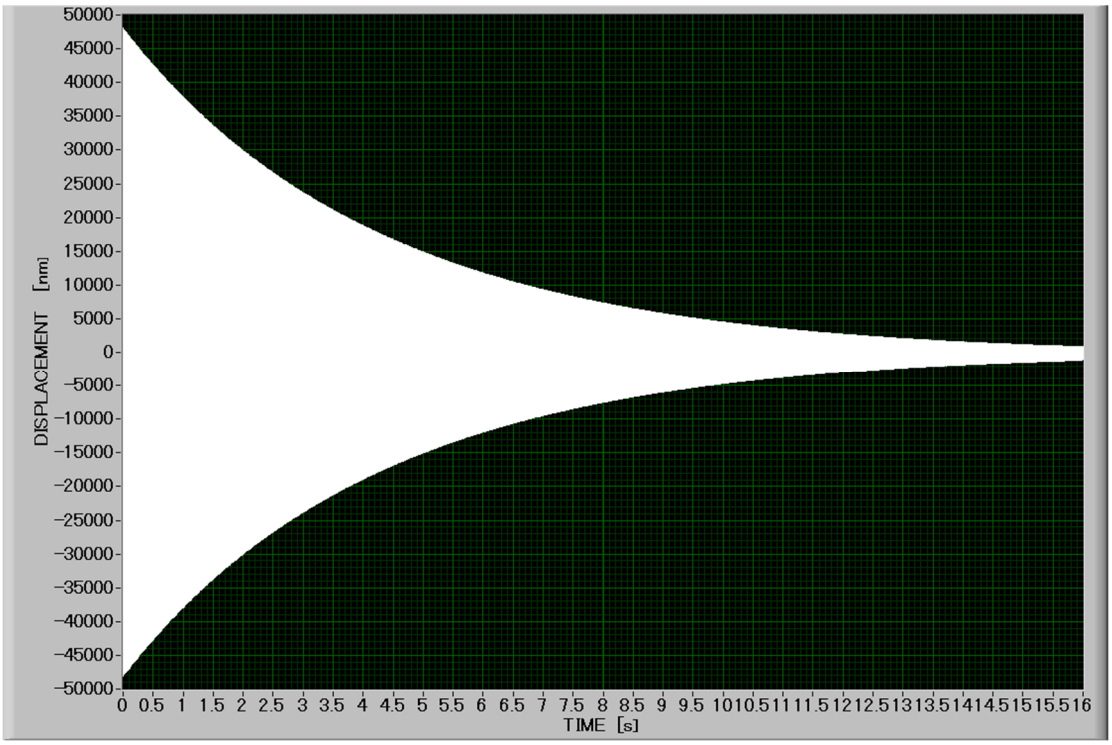
50000
45000
40000
35000
30000
25000
20000
15000
10000
5000
0
−5000
−10000
−15000
−20000
−25000
−30000
−35000
−40000
−45000
−50000
DISPLACEMENT [nm]
0 0.5 1 1.5 2 2.5 3 3.5 4 4.5 5 5.5 6 6.5 7 7.5 8 8.5 9 9.5 10 10.5 11 11.5 12 12.5 13 13.5 14 14.5 15 15.5 16
TIME [s]

Fig. 3(a)

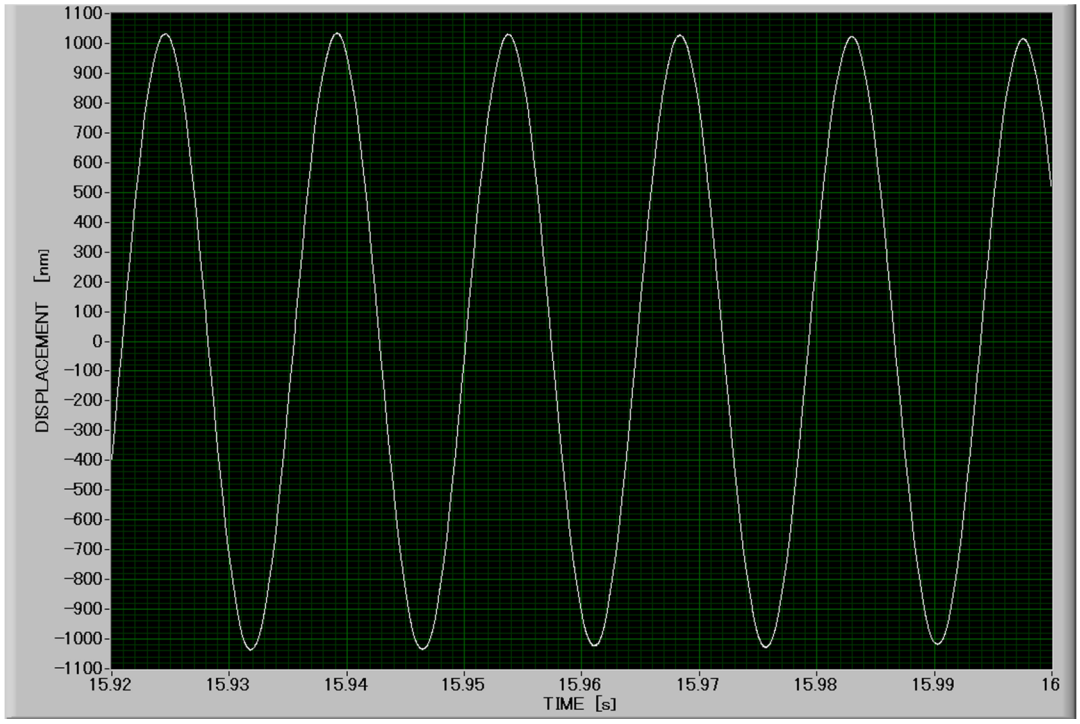
1100
1000
900
800
700
600
500
400
300
200
100
0
−100
−200
−300
−400
−500
−600
−700
−800
−900
−1000
−1100
DISPLACEMENT [nm]
15.92
15.93
15.94
15.95
15.96
15.97
15.98
15.99
16
TIME [s]

Fig. 3(b)

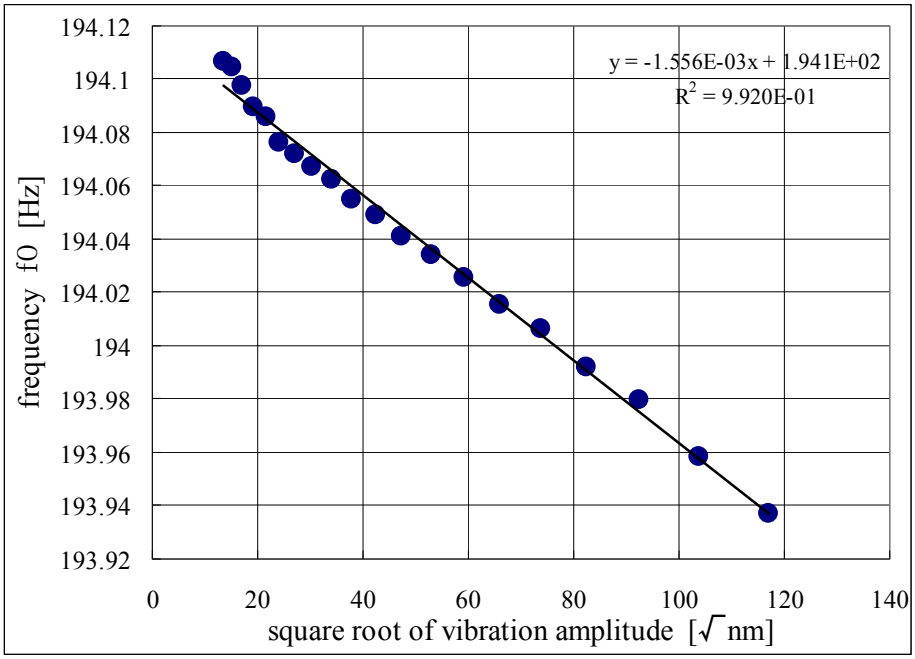
194.12
194.1
194.08
194.06
194.04
194.02
194
193.98
193.96
193.94
193.92
frequency f0 [Hz]
y = -1.556E-03x + 1.941E+02
R2 = 9.920E-01
0
20
40
60
80
100
120
140
square root of vibration amplitude [√nm]

Fig. 4

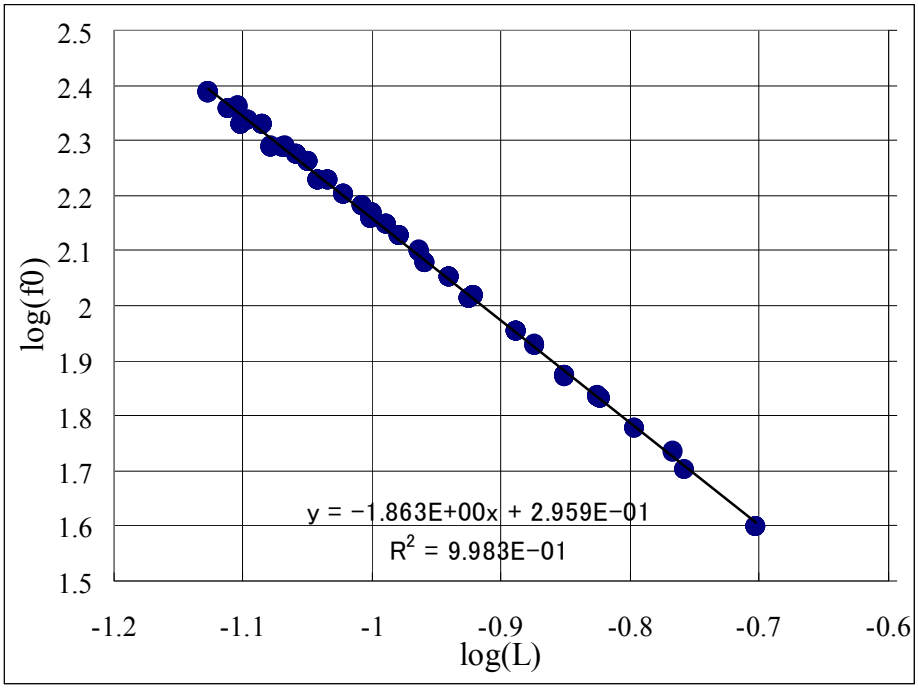
2.5
2.4
2.3
2.2
2.1
2
1.9
1.8
1.7
1.6
1.5
log(f0)
y = −1.863E+00x + 2.959E−01
R2 = 9.983E−01
-1.2
-1.1
-1
-0.9
-0.8
-0.7
-0.6
log(L)

Fig. 5

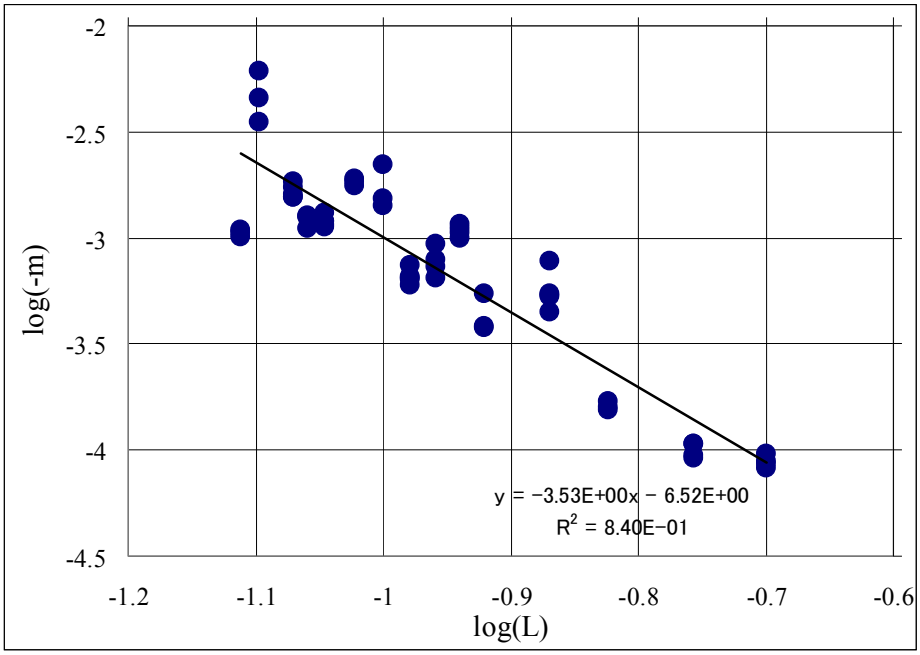
-2
-2.5
-3
-3.5
-4
-4.5
log(-m)
-1.2
-1.1
-1
-0.9
-0.8
-0.7
-0.6
log(L)
y = −3.53E+00x − 6.52E+00
R2 = 8.40E−01

Fig.6

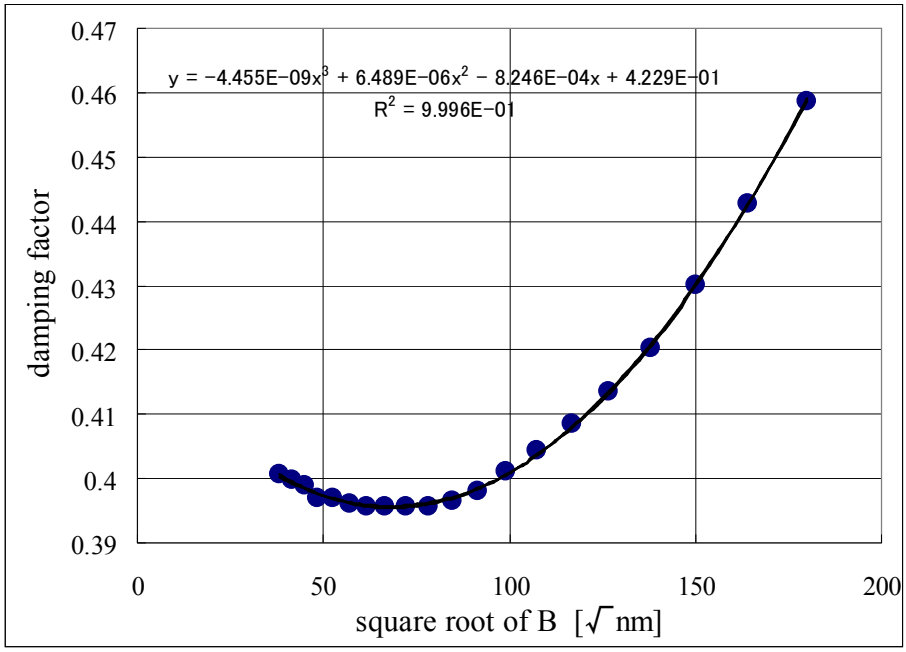
y = −4.455E−09x3 + 6.489E−06x2 − 8.246E−04x + 4.229E−01
R2 = 9.996E−01
damping factor
0.47
0.46
0.45
0.44
0.43
0.42
0.41
0.4
0.39
0
50
100
150
200
square root of B [√nm]

Fig.7

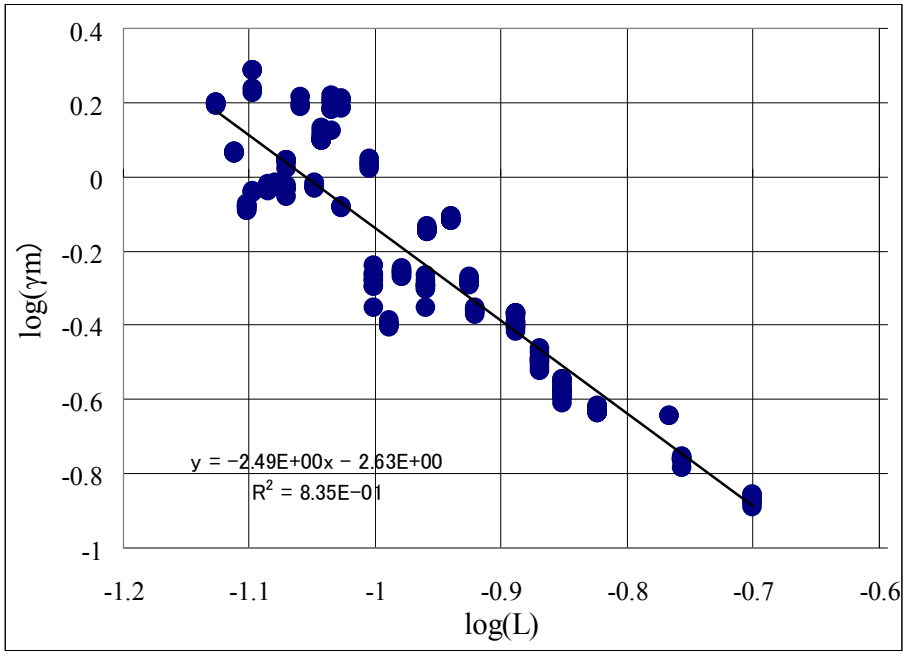
0.4
0.2
0
-0.2
-0.4
-0.6
-0.8
-1
log(γm)
y = −2.49E+00x − 2.63E+00
R2 = 8.35E−01
-1.2
-1.1
-1
-0.9
-0.8
-0.7
-0.6
log(L)

Fig. 8

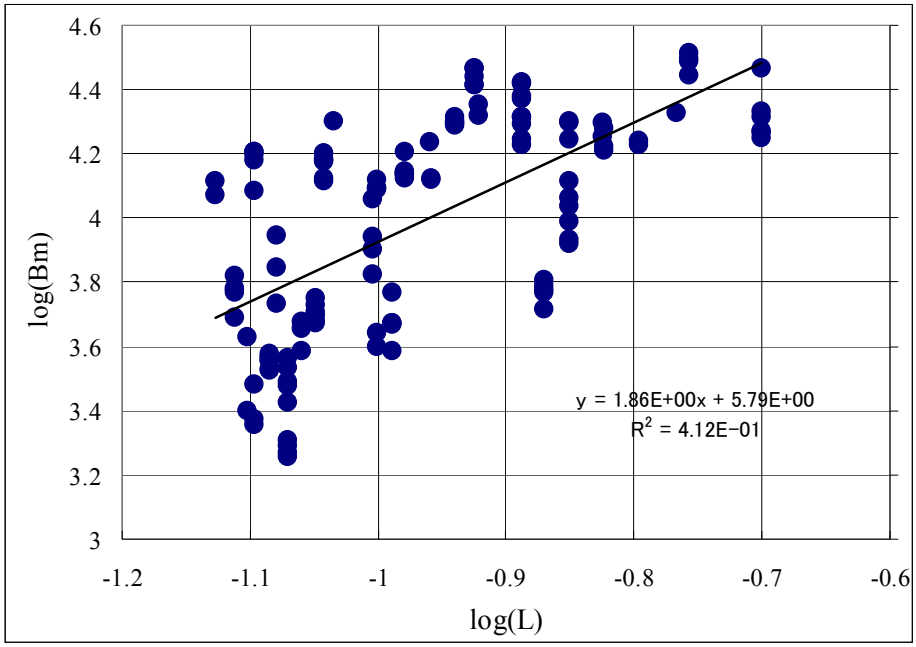
4.6
4.4
4.2
4
3.8
3.6
3.4
3.2
3
log(Bm)
-1.2
-1.1
-1
-0.9
-0.8
-0.7
-0.6
log(L)
y = 1.86E+00x + 5.79E+00
R2 = 4.12E-01

Fig. 9

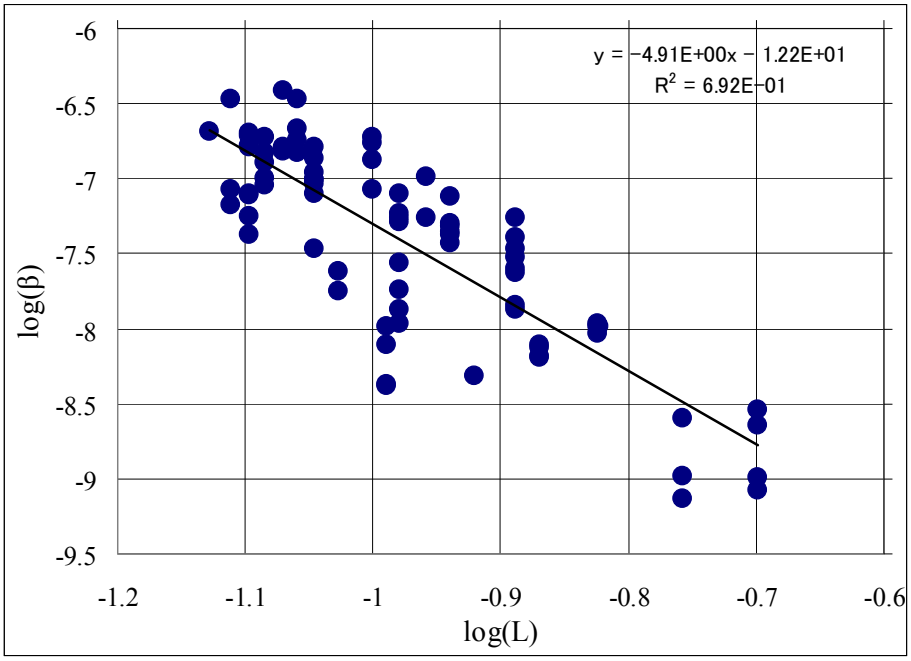
y = −4.91E+00x − 1.22E+01
R2 = 6.92E−01
-6
-6.5
-7
-7.5
-8
-8.5
-9
-9.5
log(β)
-1.2
-1.1
-1
-0.9
-0.8
-0.7
-0.6
log(L)

Fig. 10

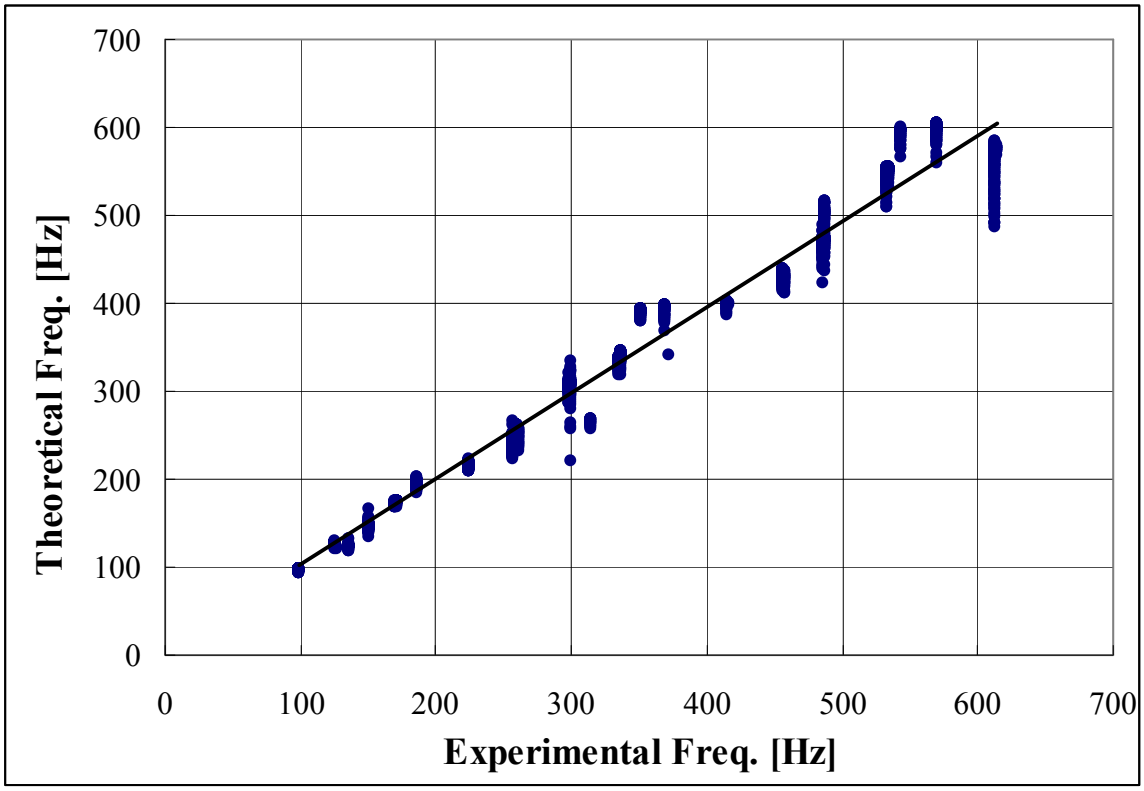
700
600
500
400
300
200
100
0
Theoretical Freq. [Hz]
0
100
200
300
400
500
600
700
Experimental Freq. [Hz]

Fig 11

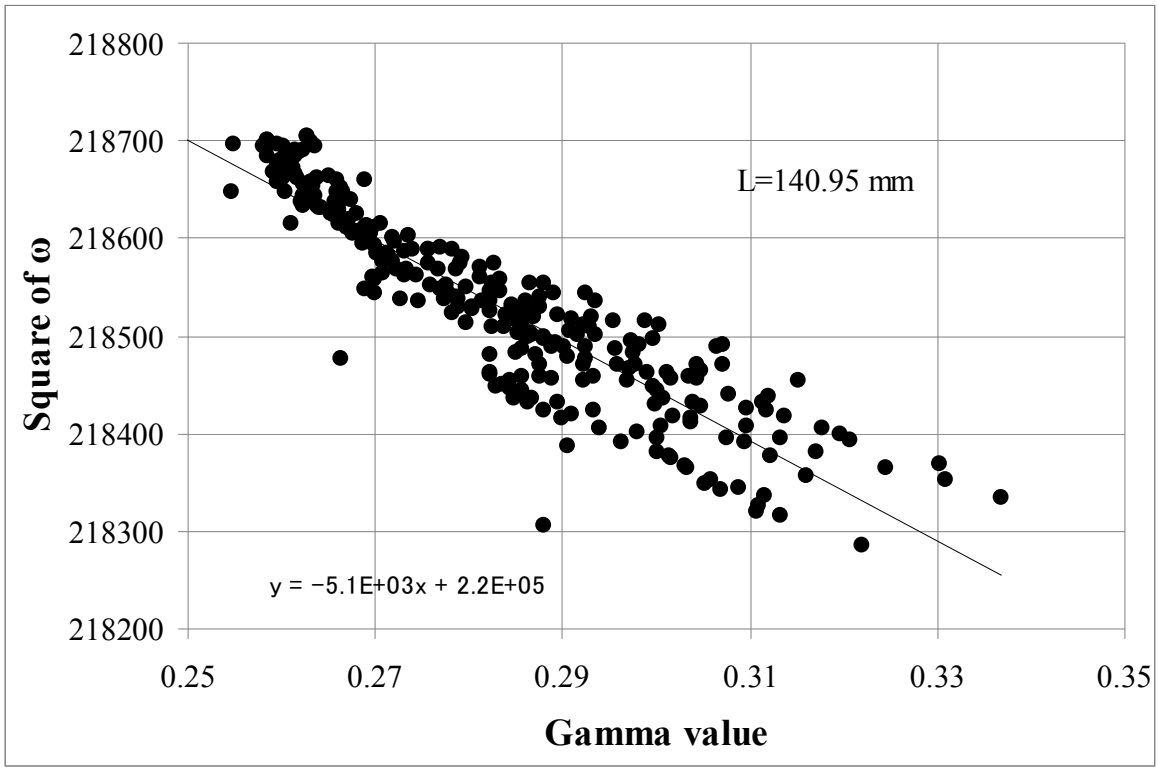
218800
218700
218600
218500
218400
218300
218200
Square of ω
L=140.95 mm
y = −5.1E+03x + 2.2E+05
0.25
0.27
0.29
0.31
0.33
0.35
Gamma value

Fig. 12